Intermittent switching for three repulsively coupled oscillators

Kentaro Ito
Department of Mathematics, Graduate School of Science, Hokkaido University, Sapporo 060-0810, Japan

Yasumasa Nishiura
Research Institute for Electronic Science, Hokkaido University, Sapporo 060-0812, Japan

(Received 20 October 2007; revised manuscript received 4 February 2008; published 28 March 2008)

We study intermittent switching behaviors in a system with three identical oscillators coupled diffusively and repulsively, to clarify a bifurcation scenario which generates such intermittent switching behaviors. We use the Stuart-Landau oscillator, which is a general form of Hopf bifurcation, and can describe both cases: limit cycle and inactive (i.e., non-self-oscillatory) cases. From a numerical study of the bifurcation structure, two different routes to chaos which has S_3 symmetry were found. One is the sudden appearance of chaos as Pomeau-Manneville intermittency, which is found for the inactive case. In this case a trajectory shows switching among three mutually symmetric tori when a parameter exceeds critical value. The other route, which appears for the limit cycle case, consists of two parts: First, chaos with lower symmetry appears through period doubling, and after the two successive attractor-merging crises, chaos which has S_3 symmetry appears. At each crisis, the attractor changes its symmetry.

DOI: 10.1103/PhysRevE.77.036224 PACS number(s): 05.45.Ac, 05.45.Xt, 82.40.Bj

I. INTRODUCTION

Coupled nonlinear oscillators show a rich variety of collective phenomena such as synchronization [1,2], clustering [3] and chaos [4], and are widely studied not only theoretically, but also experimentally [5–8]. In this regard, one area of interest is in spontaneous transitions among several states. For example, some periodic oscillating patterns which have spatiotemporal symmetry have been observed in the three coupled biological oscillators comprising the plasmodial slime mold [5,6]. In this system, slime mold shows an oscillating pattern for a long time, however, after a while it shows switching to different oscillating patterns. Similar switching behavior is also observed in a system with the three coupled oscillators in Belousov-Zhabotinsky (BZ) reaction systems [7].

One explanation of such a switching behavior is chaotic itinerancy [9]. Chaotic itinerancy is a concept to describe a dynamical behavior which shows chaotic transitions among low dimensional ordered states. The switching behavior often appears for a system with coupled chaotic elements and a system with a large number of coupled periodic elements. However, the switching behavior is less studied for a small number of coupled periodic elements. In the present paper, we propose a model with three coupled oscillators, which shows intermittent switching behaviors. We employ an idealized amplitude model for each oscillator, to investigate the relation between the appearance of switching behavior and the characteristic property for the oscillator itself. We clarify the bifurcation scenarios leading to the switching behaviors in the system by changing the intensity of amplitude dependency of the oscillators.

In most studies, collective behavior of globally coupled oscillators has been studied by using the phase model [10], because the phase model is a good approximation of coupled limit cycle oscillators for weak coupling. It is known that systems with three weakly coupled oscillators [11–13] show a rich variety of solutions. If the phase oscillators are identical [12], heteroclinic bifurcations may occur. However, the system does not show any chaotic motion if the coupling term depends only on phase difference. On the other hand, switching behaviors have been observed in three coupled biological oscillators comprised of the plasmodial slime mold [5,6] and the three coupled oscillators in BZ reaction systems [7]. In those experiments, each oscillator is periodic without coupling. Thus strong coupling and/or amplitude dependency seems to be necessary to obtain switching behavior for coupled identical limit cycle oscillators. We employ the idealized amplitude model, the Stuart-Landau oscillator, for each element because the Stuart-Landau equation has an amplitude dependency on phase velocity, and the intensity of the amplitude dependency can be controlled by a parameter β. Collective behaviors for N identical Stuart-Landau oscillators diffusively coupled have been studied [4,14]. For $N=3$, characteristic frequencies were investigated in a certain parameter range with a complex coupling constant. Transitions from periodic motion to doubly periodic motion and doubly periodic motion to chaotic motion are reported [14]. However, a detailed bifurcation structure has not been studied, and a switching behavior near the bifurcation point has also not been previously reported.

We study a system with three oscillators coupled repulsively. We call the coupling attractive if a pair of coupled oscillators prefer to have the same state variable, and repulsive if they prefer to have different state variables. Purely repulsive coupling has been less studied [3,15,16] than attractive coupling since entrainment of oscillators is one of the main interests in the field of coupled oscillators. Repulsive coupling becomes important when the sum of the state variables associated with the individual oscillators tends to keep a constant value, for example, saline oscillators [17] and slime mold oscillators [5].

To study the bifurcation structure, we follow branches of solutions by numerical continuation using AUTO [18], a software for continuation and bifurcation problems. Both for the inactive (i.e., non-self-oscillatory) case and for the limit

cycle case, we find the chaos which has S_3 symmetry, however, the routes to chaos are different. For the inactive case, chaos appears suddenly as Pomeau-Manneville intermittency, and a trajectory shows switching among three mutually symmetric tori when a parameter exceeds the critical point. On the other hand, the appearance of S_3 symmetric chaos for the limit cycle case consists of two parts: first, chaos with lower symmetry appears through period-doubling bifurcations, and two successive attractor-merging crises gives the chaos with S_3 symmetry. After the second attractor merging crisis, a trajectory shows switching among three chaotic regions. This phenomenon can be explained by crisis-induced intermittency [19]. Crisis-induced intermittency is that intermittent switching among chaotic states after interior crisis or attractor-merging crisis [19]. For crisis-induced intermittency an orbit stays near one of the old attractors which existed before the crisis for a long time, after which it abruptly switches to a region of another ruin of the old attractors.

We investigate the relation between the switching among three tori and the switching among three chaotic regions. The switching among three tori can be explained as follows. Switching among three chaotic regions appears at any parameter for S_3 symmetric chaos, and the orbit often passes through the neighborhoods of the three tori. Resident time for each chaotic region becomes short if the parameter is far from the attractor-merging crisis. On the other hand, resident time for the neighborhood of the torus becomes longer if the linear instability of the torus is small, and becomes dominant if the linear instability is sufficiently small. This situation corresponds to switching among three tori.

This paper is organized as follows. In Sec. II we show our model equations: three repulsively coupled Stuart-Landau oscillators. In Sec. III the bifurcation structure for the inactive case is investigated. Intermittent switching among the S_2 *tori* is also discussed. In Sec. IV we investigate the bifurcation structure of the S_2 *torus* solution for the limit cycle case. Period doubling routes to chaos and attractor merging crises are shown. Section V discusses the relation between the switching behaviors observed in Secs. III and IV.

II. MODEL

We consider the following coupled Stuart-Landau oscillators [10]:

$$\dot{z}_j = (\alpha + i)z_j - (1 - i\beta)|z_j|^2 z_j + \kappa \sum_{n=1}^{N} (z_n - z_j), \qquad (1)$$

where $N=3$. The variable z_j, which describes the state of the jth element, is a complex number. α is a parameter specifying the distance from the Hopf bifurcation, β represents the amplitude dependency of phase velocity, and $\kappa<0$ is the coupling strength.

In this model each oscillator is coupled to every other oscillator. Note that due to the symmetry, if one oscillating solution exists, then other oscillating solutions, obtained by permuting (z_1, z_2, z_3), also exist. We define amplitude r_j and phase θ_j as $r_j \equiv |z_j|$ and $\theta_j \equiv \arg z_j$, respectively.

Without coupling, each element z_j converges to the limit cycle whose amplitude is $\sqrt{\alpha}$ if $\alpha>0$, and settles down to the fixed point $z_j=0$ if $\alpha \leq 0$. For attractive coupling $\kappa>0$, the complete synchronized state $z_1=z_2=z_3$ is stable. The dynamics of oscillators are more complicated for repulsive coupling where $\kappa<0$. Without loss of generality, we examine $\alpha=-1$ and $\alpha=1$, both with $\beta \geq 0$.

If one of z_1, z_2, and z_3 is not 0, we can reduce the system to the one with lower dimension. Equation (1) can be rewritten as the following equation:

$$w_j = [\alpha - |w_j|^2 + i\beta(|w_j|^2 - |w_3|^2)]w_j + \kappa \sum_{n=1}^{3} \left(w_n - w_j - i w_j \frac{\mathrm{Im}\, w_n}{w_3} \right), \qquad (2)$$

where $w_j \equiv z_j e^{-i\theta_3} = r_j e^{i\phi_{j3}}$ and $\phi_{jk} \equiv \theta_j - \theta_k$. This equation consists of five real variables, because the imaginary part of ω_3 becomes 0.

Due to a shift invariance of the form $(\theta_1, \theta_2, \theta_3) \to (\theta_1 + c, \theta_2 + c, \theta_3 + c)$, steadily rotating solutions in Eq. (1) correspond to fix point solutions of Eq. (2), and quasiperiodic solutions of Eq. (1), which arise from the secondary Hopf (Neimark-Sacker) bifurcation of steadily rotating solutions, correspond to periodic solutions of Eq. (2). Hence we follow a branch of the periodic solution of Eq. (2) instead of the corresponding quasiperiodic solution of Eq. (1). In the following sections, the Hopf and secondary Hopf bifurcations are discussed, however, we omit "secondary" if there is no misunderstanding.

III. INACTIVE CASE $\alpha=-1$

Let us first consider the case of $\alpha=-1$. In this case, when there is no coupling, each element does not have a limit cycle.

A. Periodic solutions

First, we show several periodic solutions, and how they bifurcate. Figure 1 shows a phase diagram of Eq. (1) obtained by AUTO. We found roughly five types of solutions in (κ, β) parameter space and refer to these as *trivial fixed point*, *rotating*, *partial antiphase*, *quasiperiodic*, and *chaotic*. Even finer structure exists around a boundary of region II in Fig. 1 but we did not study this. A trivial fixed point $z_1=z_2=z_3=0$ is stable for $\kappa>-1/3$. For $\kappa<-1/3$, the trivial fixed point becomes unstable from the stability analysis of Eq. (1), and three types of periodic solutions, namely, stable *rotating*, unstable *partial antiphase*, and unstable *partial in-phase*, emerge from the bifurcation point of the trivial fixed point at $\kappa=-1/3$.

For general globally coupled identical elements, Theorem 4.1 from Chap. XVIII in Ref. [20] proves that rotating, partial antiphase, and partial in-phase solutions appear if the in-phase solution $(z_1=z_2=z_3)$ does not bifurcate from the Hopf bifurcation point of the trivial fixed point.

A rotating solution exists for $\kappa<-1/3$ and is stable in region II of Fig. 1. The rotating solution is obtained analytically from Eq. (1), and is written as

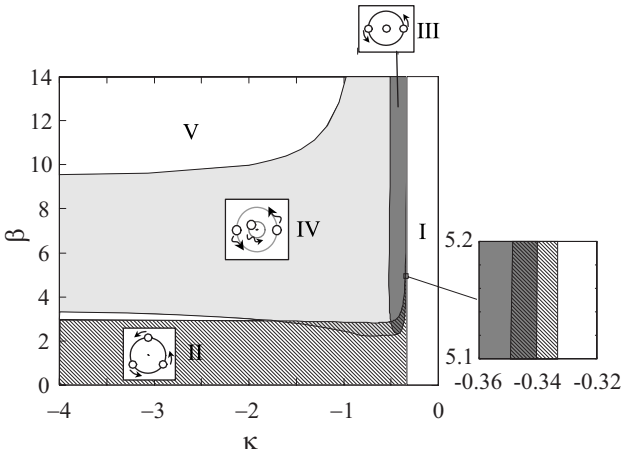

FIG. 1. A two-parameter bifurcation diagram when $\alpha=-1$. Numbered regions correspond to the following stable solutions. I: trivial fixed point; II: rotating; III: partial antiphase; IV: torus bifurcated from partial antiphase; V: chaotic. An intermittent switching solution is observed above the boundary between IV and V. The chaotic behavior is also observed in the white color region between II and IV. Where the meshed region II overlaps III and IV, both stable solutions are possible. Stable torus bifurcated from the rotating solution exists in a narrow region above the boundary of region II when $\kappa>-0.39$, but this is not illustrated here.

$$(z_1(t),z_2(t),z_3(t)) = (f(t),f(t)e^{-2\pi i/3},f(t)e^{-4\pi i/3}), \qquad (3)$$

where $f(t)\equiv \mathrm{Re}^{i((1+\beta R^2)t+\theta_0)}$, $R\equiv\sqrt{\alpha-3\kappa}$. The rotating solution becomes unstable through a secondary Hopf bifurcation. The Hopf bifurcation line is illustrated as the upper boundary of region II in Fig. 1. An unstable quasiperiodic solution emerges from the Hopf bifurcation point. An inset of Fig. 1 shows that the rotating solution is stable if κ is sufficiently near the Hopf bifurcation point $\kappa=-1/3$. Clearly the effect of amplitude dependency will be very small for the rotating solutions of Eq. (3) in this region since R will be small.

A partial antiphase solution can be written as

$$(z_1(t),z_2(t),z_3(t)) = (0,f(t),-f(t)). \qquad (4)$$

A partial antiphase solution is stable in region III. Note that region III is not in contact with region I in Fig. 1. A partial antiphase solution is unstable if κ is sufficiently near $-1/3$ as shown in the inset of Fig. 1. The boundary of region III corresponds to secondary Hopf bifurcation points of the partial antiphase solution.

A partial in-phase solution is a periodic solution in which two elements have the same position, i.e., $z_i=z_j$. A partial in-phase solution exists if $\kappa<-1/3$ and is always unstable.

B. First route to S_3 chaos: From S_2 torus to S_3 chaos

A quasiperiodic solution appears in region IV in Fig. 1. The boundary line between region III and region IV is the secondary Hopf bifurcation point of the partial antiphase solution. Decreasing κ from region III to region IV, a new oscillation mode appears. A time series of the quasiperiodic solution near the Hopf bifurcation point is shown in Figs.

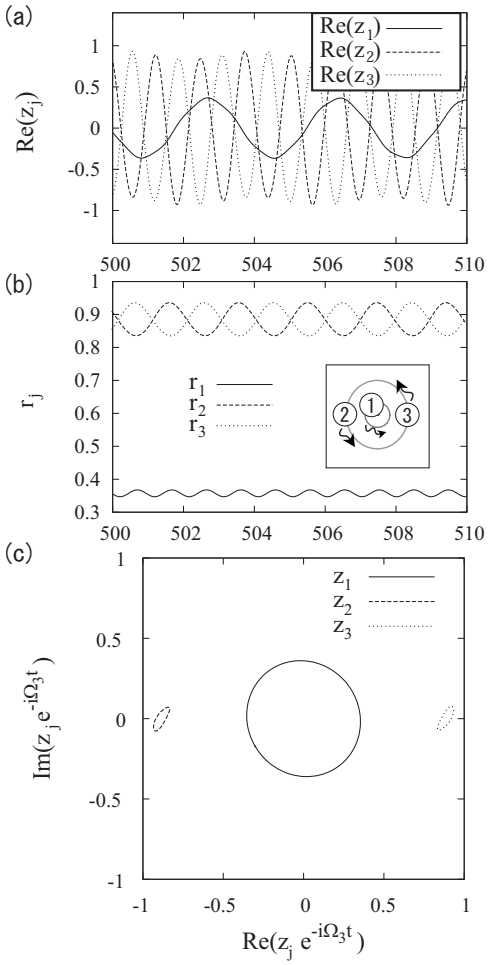

FIG. 2. An example of an S_2 torus solution in region IV, where $\kappa=-0.6$, $\beta=5.0$. (a) Time series of $\mathrm{Re}(z_j)$, (b) time series of amplitude $|z_j|$, and (c) orbits of oscillators in rotating coordinates. This solution corresponds to a quasiperiodic solution in coordinates $(r_1,r_2,r_3,\theta_1,\theta_2,\theta_3)$.

2(a) and 2(b). Figure 2(a) shows that two elements oscillate with large amplitude with time period T. The orbit of the solution on a coordinate which is rotating with Ω_3 is shown in Fig. 2(c), where Ω_i is the mean phase velocity of θ_i. Figure 2(c) shows that the phase difference between them is around π. It can also be seen from Fig. 2(a) that the other element with smaller amplitude oscillates with a different frequency. The mean phase velocities for elements obey the following relations: $\Omega_1=\Omega_3-2\pi/T$ and $\Omega_2=\Omega_3$. The periods T and $2\pi/\Omega_3$ are the characteristic periods for the quasiperiodic solution.

Although this solution is quasiperiodic in fixed coordinates (z_1,z_2,z_3), Fig. 2 shows that amplitude r_j and phase difference ϕ_{ij} of the quasiperiodic solution oscillate periodically. This is related to the fact that the partial antiphase solution corresponds to a fixed point in Eq. (2), as mentioned in the previous section. The quasiperiodic solution corresponds to a periodic solution of Eq. (2), and the period of the this solution is same as the one of (r_1,r_2,r_3) [Fig. 2(b)]. From a viewpoint of symmetry, Fig. 2(b) shows that r_2, r_3 oscillate at a time period of T with a half-period time lag, and

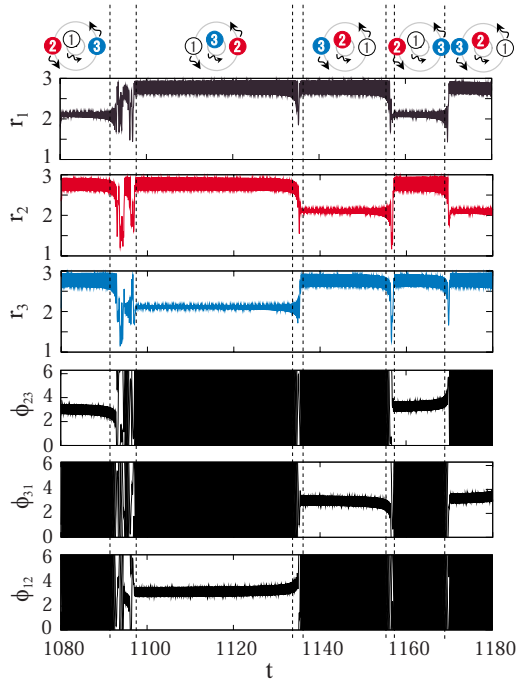

FIG. 3. (Color online) Times series of r_1, r_2, r_3, ϕ_{23}, ϕ_{31}, and ϕ_{12}, with $\alpha=-1$, $\kappa=-3$, and $\beta=9.8$. The vertical line represents the start and end time of each laminar state. A schematic illustration of each state is shown above the time series. The two elements oscillating with largest amplitude are always almost antiphase. The switching among the three S_2 tori appears to be random.

r_1 oscillates at a period of $T/2$. The attractor is invariant under permutation (z_1, z_3) and so we refer to the attractor as an S_2 torus for convenience. S_n represents the symmetric group consisting of all permutations of n elements. The S_2 torus solution is stable in region IV and becomes unstable in region V as β passes through the boundary between regions IV and V due to a subcritical pitchfork bifurcation at the boundary.

A chaotic solution emerges in the region illustrated as region V in Fig. 1. A time series of the chaotic solution is illustrated in Fig. 3. Figure 3 shows intermittent switching among three states, each of which corresponds to an unstable S_2 torus. The switching behavior is as follows. One element oscillates in a small amplitude orbit for a long time. At the end of this time the element leaves the small amplitude orbit and another element takes its place. In other words, the trajectory exhibits intermittent switching among three S_2 tori in phase space. The trajectory often visits the same S_2 torus in succession, however, the order in which the S_2 tori are visited seems random.

C. Average laminar length

We study the average laminar length of the switching solution close to the critical point β_c. The average laminar length $\langle l \rangle$ of this intermittency scales as follows [21]:

$$\langle l \rangle \propto (\beta - \beta_c)^{-\gamma} \tag{5}$$

for β close to the critical bifurcation point β_c. The scaling factor γ is called a critical exponent. We adopt a surface $r_2 = r_3$ as a Poincaré section and plot the point (w_1, w_2, w_3) when the trajectory crosses it with $\dot{r}_3 - \dot{r}_2 > 0$. We call that the system is in the laminar state when it is in a certain neighborhood of the unstable S_2 torus. The result of numerical simulation depicted in Fig. 4 shows $\gamma \simeq 1$. In general, intermittency was distinguished by the three types of bifurcation points [22]: type I, saddle node bifurcation; type II, subcritical Hopf bifurcation; and type III, subcritical period-doubling bifurcation. These types of intermittency are known as Pomeau-Manneville intermittency. The critical exponent γ is 0.5 for type I intermittency and 1 for type II and type III intermittencies. In this case the critical bifurcation point is a subcritical pitchfork bifurcation of the S_2 torus solution. The intermittency after the pitchfork bifurcation does not belong to type I, II, or III. However, we can apply the analysis of type III intermittency to our system. In general, if period-doubling bifurcation takes place for a one-dimensional map M, the pitchfork bifurcation takes place for the two times iterated map M^2. Therefore the probability distribution for the laminar length can be estimated by the same procedure as for type III intermittency [23], which gives $\gamma=1$. This value of γ matches the result of our numerical experiment. From the viewpoint of symmetry, a chaotic attractor which corresponds to the switching trajectory has S_3 symmetry; invariant from permutation (z_1, z_2, z_3). We call the S_3 symmetric chaotic attractor S_3 chaos for convenience. In this section we observed the following route to chaos: trivial fixed point $\rightarrow$ partial antiphase $\rightarrow S_2$ torus $\rightarrow S_3$ chaos. In the next section we discuss the structure of S_3 chaos for $\alpha=1$.

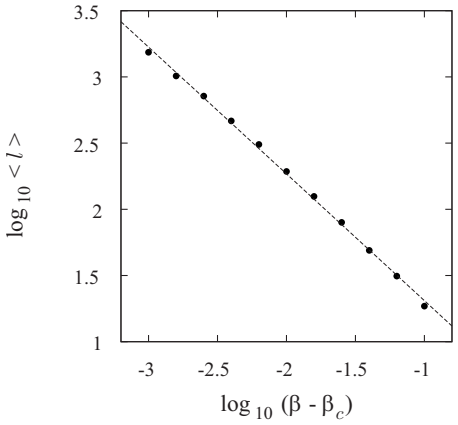

FIG. 4. Dependence of the average laminar length $\langle l \rangle$ for $\kappa=-5.0973$, $\beta_c=9.4593$. The laminar length is defined as the duration over which the distance from an S_2 torus does not exceed a certain threshold on the Poincaré section. Here we choose 0.05 as the threshold value. The solid line indicates the linear fitting which yields a critical exponent $\gamma=0.96$.

IV. LIMIT CYCLE OSCILLATOR CASE $\alpha=1$

In this section we consider the case of $\alpha=1$. For $\alpha=1$, each element has a limit cycle when there is no coupling term. We will discuss other switching behaviors which show switching among chaotic states. We define the S_1 torus as a torus which is not invariant for any permutation of (z_1, z_2, z_3)

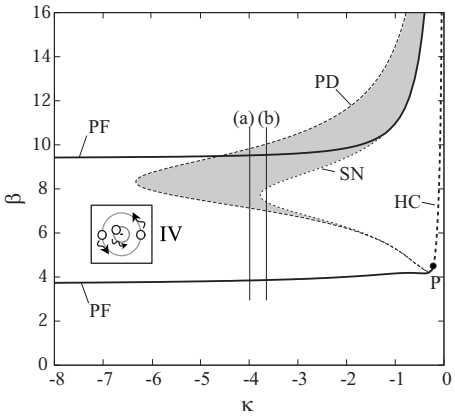

FIG. 5. A two-parameter bifurcation diagram of the S_2 torus solution for $\alpha=1$. A stable S_2 torus exists in region IV which is located between solid lines representing pitchfork bifurcation points. The gray region represents a region where stable S_1 tori exist. Stable S_2 tori and S_1 tori coexist in the overlapped region. The bifurcation points are denoted as follows: PF, pitchfork bifurcation of S_2 torus; SN, saddle-node bifurcation of S_1 torus; PD, period-doubling bifurcation of S_1 torus; HC, heteroclinic bifurcation. There is a region near HC with large β, on whose boundary the S_2 torus solution bifurcates. However, the region is not illustrated here because we did not study it in any detail.

except the identity permutation. The S_1 torus is bifurcated from the symmetry breaking pitchfork bifurcation of the S_2 torus. To show the second route to the switching behavior, we focus on bifurcations of the S_2 torus, S_1 torus, and chaotic attractors originating from the S_1 torus.

A. Bifurcations from S_2 torus to S_1 torus

First, we follows a branch of S_2 torus which is the start point of the route to chaos. Figure 5 shows a two-parameter bifurcation diagram for the S_2 torus. The S_2 torus is stable in region IV, and was obtained by following the S_2 torus solution from $\alpha=-1$ to $\alpha=1$. Unlike the result for $\alpha=-1$, there is no secondary Hopf bifurcation point which generates an S_2 torus for $\alpha=1$. Furthermore, trivial fixed point and partial antiphase solutions are unstable at any (κ,β). Before we discuss the detail of the bifurcation structure, we make some comments on the solutions which are not related to this route. We note that the other types of stable solutions, rotating solution described in Eq. (3) and quasiperiodic solution bifurcated from the rotating solution, also exist in a part of the parameter space shown in Fig. 5. A trajectory of the quasiperiodic solution is on a torus which is invariant under a cyclic permutation (i.e., Z_3 symmetric). We confirm that those periodic and quasiperiodic solutions, except for the S_1 torus, are unstable above the upper boundary of region IV, which is labeled PF in Fig. 5, by following the branches numerically.

We consider the bifurcation structure of an S_2 torus which is invariant under a permutation (z_2,z_3). If β is increased from within region IV then the S_2 torus becomes unstable when β passes through the pitchfork bifurcation point of the S_2 torus. The pitchfork bifurcation points correspond to the

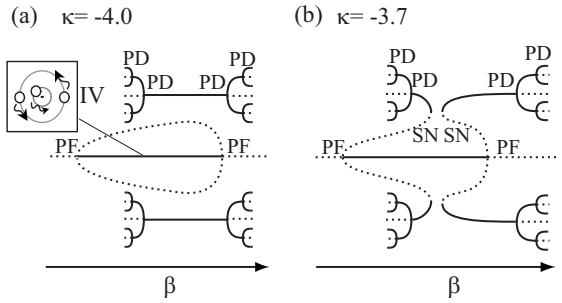

FIG. 6. A schematic illustration of the bifurcation diagram of the S_2 torus solution for (a) $\kappa=-4.0$, (b) $\kappa=-3.7$. The solid lines and dotted lines represent stable and unstable branches, respectively. The horizontal line on which PF points exist represents the S_2 torus branch. The choices of κ here correspond to the lines labeled (a), (b) in Fig. 5.

upper solid boundary line of region IV in Fig. 5. The lower solid boundary line to the left of point P is also a pitchfork bifurcation line of the S_2 torus. The pitchfork bifurcation line on the upper boundary is supercritical for $\kappa>-1.19$ and subcritical for $\kappa<-1.19$. A region where stable S_1 tori exist is illustrated by the gray region in Fig. 5. For $\kappa>-1.19$ stable S_1 tori bifurcate from the supercritical pitchfork bifurcation points, whereas for $\kappa<-1.19$ the branches are unstable. For $-3.76<\kappa<-1.19$ [Fig. 6(b)], the branches of unstable S_1 tori fold and become stable from saddle-node bifurcations. For $\kappa<-3.76$ [Fig. 6(a)], branches of S_1 tori, which bifurcated from the upper boundary line of region IV, connect to the branch which bifurcated from the lower solid boundary.

A boundary labeled HC exists above the point P. Here we mention about the S_2 torus near the boundary labeled HC in Fig. 5 only briefly. As κ approaches to HC from the left, the S_2 torus approaches two unstable partial in-phase solutions, and the trajectory spends increasingly longer times passing through the neighborhoods of partial in-phase solutions. For example, if the S_2 torus is invariant under a permutation (z_2,z_3), the orbit approaches two unstable solutions; one is characterized by $z_1=z_2$ and the other one is characterized by $z_1=z_3$. On reaching HC the S_2 torus becomes a heteroclinic cycle connecting the pair of partial in-phase solutions.

B. Period doubling route to S_1 chaotic attractor

We investigate the bifurcation diagram of a stable S_1 torus at $\kappa=-3.7$ (Fig. 7). As β is increased period-doubling bifurcations occur on a stable S_1 torus branch. The first period-doubling bifurcation line (PD) is illustrated in Fig. 5. An inset of Fig. 7 shows that the stable S_1 torus develops into a chaotic attractor after period-doubling bifurcations. We call this attractor, which is not invariant for any permutation of (z_1,z_2,z_3) except the identity permutation, an S_1 chaotic attractor for convenience.

C. Attractor-merging crisis I: From S_1 chaotic attractors to S_2 chaotic attractor

Although each S_1 chaotic attractor is not symmetric itself, a pair of S_1 chaotic attractors which originally bifurcated

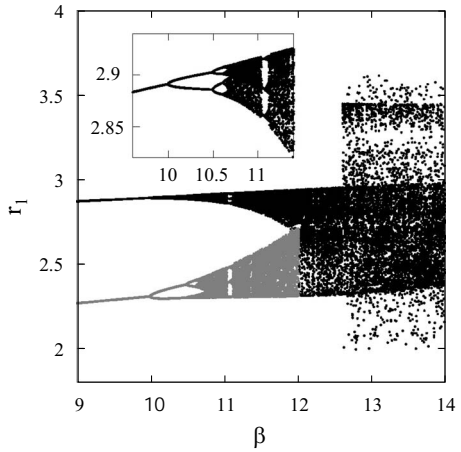

FIG. 7. Bifurcation diagram of an S_1 torus on a Poincaré section $r_2=r_3$ for $\alpha=1.0$, $\kappa=-3.7$, $\beta_1=12.017\,74$, and $\beta_2=12.611$. Points on the section are plotted only if $\dot{r}_3-\dot{r}_2>0$. For $\beta<\beta_1$, black dots and gray dots represent the different attractors which originally bifurcated from the same S_2 *torus*. The two attractors merge into an S_2 chaotic attractor at β_1. Three S_2 chaotic attractors merge into one S_3 chaos at β_2 which is accompanied by a sudden widening. Note that the other two S_2 chaotic attractors are not plotted for $\beta<\beta_2$.

from the same S_2 torus is mutually symmetric, because of the symmetry of the system. The total number of S_1 chaotic attractors is 6 since three pairs exist. Increasing β, the distance between a pair of S_1 chaotic attractors decreases until the distance goes to zero and a crisis occurs at β_1. Figure 8 shows two S_1 chaotic attractors simultaneously colliding with an S_2 torus which is on the basin boundary between them, as β passes through β_1. As β exceeds the critical value β_1, the two mutually symmetric S_1 chaotic attractors will merge into one attractor which has S_2 symmetry: invariant under a permutation of (z_2,z_3). This type of global bifurcation is called an attractor-merging crisis [19].

The attractor-merging crisis induces intermittent switching between two chaotic attractors which exist before the crisis. The trajectory spends a long time τ in a region where the attractor existed before the crisis. After this time the orbit

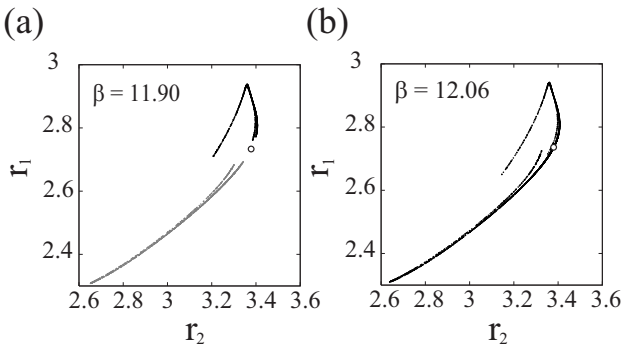

FIG. 8. Phase portrait of (a) S_1 chaotic attractors and (b) S_2 chaotic attractor on the Poincaré section $z_1=z_2$ for $\alpha=1$, $\kappa=-3.7$. Points on the section are plotted only if $\dot{r}_3-\dot{r}_2>0$. A white disk represents an unstable S_2 *torus*. Two S_1 chaotic attractors touch the S_2 torus at $\beta=\beta_2$ and an attractor-merging crisis occurs.

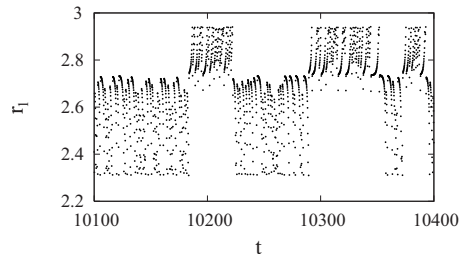

FIG. 9. Time series of an S_2 chaotic attractor on the Poincaré section $z_1=z_2$ at $\alpha=1$, $\kappa=-3.7$, and $\beta=12.06$. Points on the section are plotted only if $\dot{r}_3-\dot{r}_2>0$. Intermittent switching among two states is clearly shown.

moves to the region where the other attractor previously existed. Figure 9 shows intermittent switching among two chaotic states. It can be seen that each chaotic state consists of short laminar phases, which stay near one of the two original S_2 tori branches, and burst phases. This property persists even when β is not near β_1. Figure 10 shows that the average transient lifetime $\langle\tau\rangle$ scales as follows:

$$\langle\tau\rangle \propto (\beta-\beta_1)^{-\nu} \tag{6}$$

for β close to β_1.

D. Attractor-merging crisis II: From S_2 chaotic attractors to S_3 chaos

Since this system has S_3 symmetry, there are three isolated S_2 chaotic attractors for $\beta_1<\beta<\beta_2$. As β exceeds β_2, the three mutually symmetric attractors are replaced by one large S_3 symmetric attractor, which is invariant to permutation (z_1,z_2,z_3). We refer to the large S_3 symmetric attractor as S_3 chaos as in the previous section.

For β slightly larger than β_2, the trajectory of S_3 chaos shows intermittent switching among the three S_2 chaotic regions which correspond to S_2 chaotic attractors before the crisis, as shown in Fig. 11. $\langle\tau_2\rangle$ which represents the average lifetime of an S_2 chaotic region, becomes smaller with in-

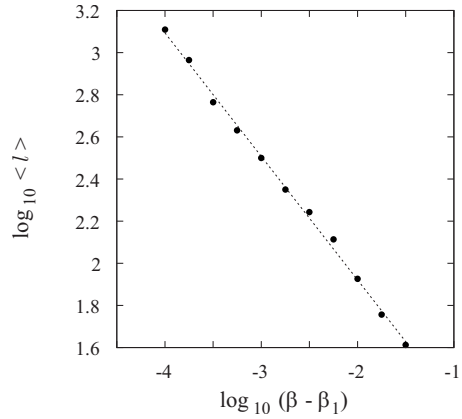

FIG. 10. Dependence of the average lifetime $\langle\tau\rangle$ with $\beta_1=12.017\,74$. The dotted line indicates the linear fitting which yields a critical exponent $\nu=-0.59$.

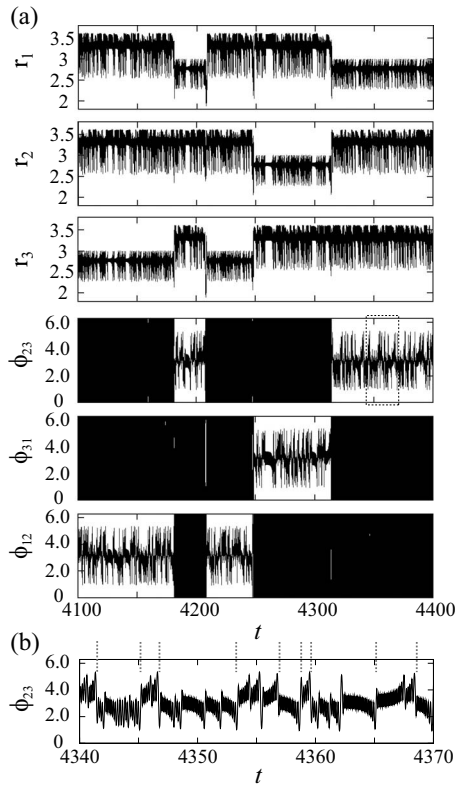

FIG. 11. (a) Time series of r_1, r_2, r_3, ϕ_{23}, ϕ_{31}, and ϕ_{12}, with $\alpha=1.0$, $\kappa=-3.7$, and $\beta=12.64$. The switching among the three S_2 chaotic attractors seems random. (b) An enlargement of the time series of ϕ_{23}. The times at which switching occurs between S_1 chaotic regions are illustrated by the dotted lines.

creasing $\beta-\beta_2$. When the trajectory is in an S_2 chaotic region, it shows switching among two S_1 chaotic regions, and frequently passes near the S_2 torus which exists between them, just as the trajectory on an S_2 chaotic attractor did. Note that these properties of the switching behavior are also observed if β is substantially larger than β_2.

E. Symmetry transitions

To investigate how the symmetry of the attractor changes through the bifurcation diagram, we focus the following properties of the symmetry: For S_3 chaos, $\langle r_1\rangle=\langle r_2\rangle=\langle r_3\rangle$ holds. On the other hand, for S_2 chaos and torus, there exists j, k, and l with $j\neq k$ and $k\neq l$ such that $\langle r_j\rangle=\langle r_k\rangle\neq\langle r_l\rangle$. We introduce the order parameters $P_1\equiv|\langle r_1+r_2e^{2\pi i/3}+r_3e^{4\pi i/3}\rangle|$ and $P_2\equiv|\langle r_1-r_2\rangle\langle r_2-r_3\rangle\langle r_3-r_1\rangle|$. P_1 becomes 0 if the attractor is invariant under any permutation of elements. Therefore P_1 is assumed to be the index of S_3 symmetry for the attractor. P_2 becomes 0 if the attractor is invariant under a permutation of one pair of elements (z_j,z_k), therefore P_2 is assumed to be the index of S_2 symmetry. For S_n chaotic attractors, P_1 and P_2 obey the following relations:

$$S_3 \text{ chaos: } P_1=0,\ P_2=0,$$

$$S_2 \text{ chaotic attractor: } P_1\geq 0,\ P_2=0,$$

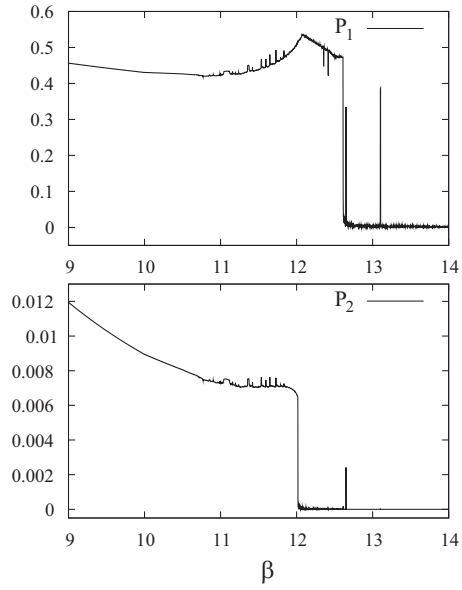

FIG. 12. P_1, P_2 vs β for $\alpha=1.0$, $\kappa=-3.7$. $P_2=0$ if the attractor has S_2 symmetry, and $P_1=P_2=0$ if the attractor has S_3 symmetry. P_1 and P_2 are calculated from time series from $t=100$ to $t=100\ 100$.

$$S_1 \text{ chaotic attractor: } P_1\geq 0,\ P_2\geq 0, \tag{7}$$

Figure 12 shows that P_1 jumps down to 0 as β exceeds β_2, and P_2 jumps down to 0 as β exceeds β_1. This results imply that the symmetry of attractor changes from S_1 to S_2 as β exceeds β_1, and from S_2 to S_3 and as β exceeds β_2, respectively. Sharp peaks of P_1 and P_2 correspond to windows of the bifurcation diagram as shown in Fig. 12. For example, S_1 and S_2 symmetric tori appear at $\beta=12.650,\ 13.102$, respectively.

V. DISCUSSION

We have presented several oscillating patterns and switching behaviors in three repulsively coupled Stuart-Landau equations. The number of the dimensions for our model is essentially 5. This model could be one of the simplest models which shows intermittent switching among three and more states. For sufficiently small β, the rotating solution is the only stable solution. For large β, S_2 torus and chaotic solutions appear. Our result implies that chaotic element and external noise are not necessary for the switching behaviors. For three globally coupled identical oscillators, it can be said that spontaneous switching behavior may occur when the amplitude dependency and repulsive coupling are sufficiently strong.

We reported two different routes to S_3 chaos for large β. One route is S_2 torus$\rightarrow S_3$ chaos for $\alpha=-1$ [Fig. 13(b)]. In this route, intermittent switching among three S_2 tori are observed, and the average time between bursts scales as a power law in the difference of a parameter from its critical value. The other route consists of two parts. The first part is the creation of chaotic attractors through the period-doubling cascade: S_2 torus$\rightarrow S_1$ torus$\rightarrow S_1$ chaotic attractor. The second part is two successive attractor-merging crises: S_1 cha-

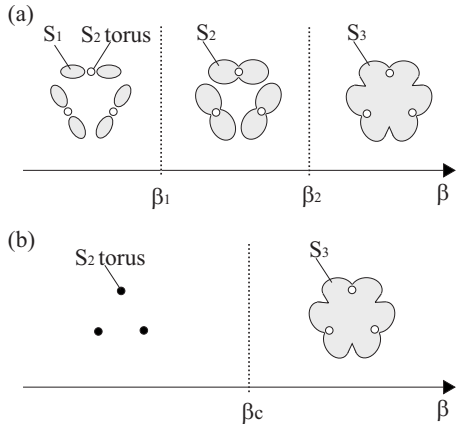

FIG. 13. Schematic illustration of bifurcations to S_3 chaotic attractor: Gray regions labeled S_1, S_2, S_3 are chaotic attractors. A black disk represents a stable S_2 torus, and a white disk represents an unstable S_2 torus.

otic attractor $\rightarrow S_2$ chaotic attractor $\rightarrow S_3$ chaos, for $\alpha=1$ [Fig. 13(a)].

In the first route to S_3 chaos we found that the time series of an S_3 chaotic attractor showed switching among three laminar states near the pitchfork bifurcation point of the S_2 torus. Each laminar state corresponds to the neighborhood of an S_2 torus. In each laminar state, one element oscillates with a small amplitude and the other two elements oscillate with a large amplitude. We can explain the intermittent switching among S_2 tori (Fig. 3) as follows. We are far from the parameter regime where S_2 chaotic attractors merge into S_3 chaos. The trajectories therefore easily switch among S_2 chaotic regions. On the other hand, from the weak linear instability of the S_2 torus, the average lifetime of a laminar state which corresponds to an S_2 torus becomes large near the pitchfork bifurcation point. Due to the structure of the S_2 chaotic region that contains the S_2 torus, the laminar state therefore becomes dominant in each S_2 chaotic region and it is also dominant in the time series (Fig. 3) if the set of parameters is sufficiently near the bifurcation point.

To show the continuity of S_3 chaos from $\alpha=-1$ to $\alpha=1$, we perform the following transformation. If $\alpha-3\kappa>0$, Eq. (1) can be transformed to the following form:

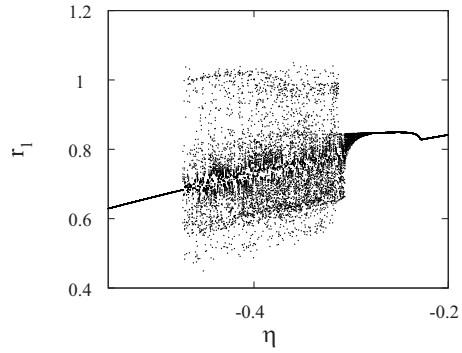

FIG. 14. Bifurcation diagram of an S_2 torus on the Poincaré section $|Z_2|=|Z_3|$ at $\beta=12.0$. We choose the same initial value for every η. The regions $\eta<-1/3$ and $\eta>-1/3$ correspond to $\alpha=-1$ and $\alpha=1$, respectively. $\eta\rightarrow-1/3$ corresponds to $\kappa\rightarrow-\infty$.

$$\frac{dZ_j}{dt'}=\left(1+\frac{i\kappa}{\eta}\right)Z_j-(1-i\beta)|Z_j|^2Z_j+\eta\sum_{n=1}^{N}Z_n, \qquad (8)$$

where $Z_j\equiv\sqrt{\alpha-3\kappa}z_j$, $t'\equiv(\alpha-3\kappa)t$, $\eta\equiv\kappa/(\alpha-3\kappa)$. $\eta<-1/3$ corresponds to $\kappa<-1/3$ at $\alpha=-1$, and $\eta>-1/3$ corresponds to $\kappa<0$ at $\alpha=1$. $\eta=-1/3$ corresponds to the limit $\kappa\rightarrow\infty$ at $\alpha=\pm1$. Figure 14 shows a one-parameter bifurcation diagram of an S_2 torus at $\beta=12.0$. It shows two routes to the onset of S_3 chaos which then seems to be continuous within the intermediate region.

As mentioned in Sec. II, for the S_2 torus, one element oscillates with smaller amplitude, and the other two elements oscillate with larger amplitude. This type of separation of elements is an important role in our system. The study of whether separation of elements has an important role for coupled N oscillator systems, and detailed global bifurcation analyses of these systems, will be interesting future work.

ACKNOWLEDGMENTS

The authors thank H. Kori and T. Ichinomiya for fruitful discussions and careful reading of this manuscript. They also thank Y. Kuramoto and A. Takamatsu for valuable discussions.

[1] A. Pikovsky, M. Rosenblum, and J. Kurths, *Synchronization: A Universal Concept in Non-linear Sciences* (Cambridge University Press, Cambridge, England, 2001).
[2] S. C. Manrubia, A. Mikhailov, and Z. H. Zanette, *Emergence of Dynamical Order* (World Scientific, Singapore, 2004).
[3] K. Okuda, Physica D **63**, 424 (1993).
[4] N. Nakagawa and Y. Kuramoto, Physica D **75**, 74 (1994).
[5] A. Takamatsu, R. Tanaka, H. Yamada, T. Nakagaki, T. Fujii, and I. Endo, Phys. Rev. Lett. **87**, 078102 (2001).
[6] A. Takamatsu, Physica D **223**, 180 (2006).
[7] M. Yoshimoto, K. Yoshikawa, and Y. Mori, Phys. Rev. E **47**, 864 (1993).
[8] I. Z. Kiss, Y. Zhai, and J. L. Hudson, Phys. Rev. Lett. **94**, 248301 (2005).
[9] K. Kaneko and I. Tsuda, Chaos **13**, 926 (2003).
[10] Y. Kuramoto, *Chemical Oscillations, Waves, and Turbulence* (Springer, Berlin, 1984).
[11] C. Baesens, J. Guckenheimer, S. Kim, and R. S. Mackey, Physica D **49**, 387 (1991).
[12] P. Ashwin, G. P. King, and J. W. Swift, Nonlinearity **3**, 585 (1990).
[13] P. Ashwin, O. Burylko, and Y. Maistrenko, Physica D **237**, 454 (2008).
[14] T. Yamada and H. Fujisaka, Z. Phys. B **28**, 239 (1977).

[15] H. Daido, Phys. Rev. Lett. **68**, 1073 (1992).
[16] L. S. Tsimring, N. F. Rulkov, M. L. Larsen, and M. Gabbay, Phys. Rev. Lett. **95**, 014101 (2005).
[17] K. Yoshikawa, N. Oyama, M. Shoji, and S. Nakata, Am. J. Phys. **59**, 137 (1991).
[18] E. J. Doedel, R. C. Paffenroth, A. Champneys, T. Fairgrieve, Y. Kuznetsov, B. Oldeman, B. Sandstede, and X. Wang, Auto2000:continuation and bifurcation software for ordinary differential equations (with homcont), 2002, http://cmvl.cs.concordia.ca/auto/
[19] C. Grebogi, E. Ott, F. Romeiras, and J. A. Yorke, Phys. Rev. A **36**, 5365 (1987).
[20] M. Golubitsky, I. Stewert, and D. G. Schaeffer, *Singularities and Groups in Bifurcation Theory* (Springer-Verlag, Berlin, 1988), Vol. II.
[21] E. Ott, *Chaos in Dynamical Systems*, 2nd ed. (Cambridge University Press, Cambridge, England, 2002).
[22] Y. Pomeau and P. Manneville, Commun. Math. Phys. **74**, 189 (1980).
[23] M. Dubois, M. A. Rubio, and P. Berge, Phys. Rev. Lett. **51**, 1446 (1983).